

**IMPROVEMENT OF STRUCTURAL DESIGN OF
AlGa_N/Ga_N BASED HEMT FOR HIGH
PERFORMANCE POWER DEVICES**

MUHAIMIN HAZIQ BIN MIHAT

UNIVERSITI SAINS MALAYSIA

2025

**IMPROVEMENT OF STRUCTURAL DESIGN OF
AlGaN/GaN BASED HEMT FOR HIGH
PERFORMANCE POWER DEVICES**

by

MUHAIMIN HAZIQ BIN MIHAT

**Thesis submitted in fulfilment of the requirements
for the degree of
Doctor of Philosophy**

February 2025

ACKNOWLEDGEMENT

I would like to express my sincere gratitude to my supervisor, Assoc. Prof. Ts. Dr. Mohd Syamsul, for his invaluable guidance, steadfast support, and mentorship throughout this research journey. His patience and consistent encouragement have helped to shape this thesis and inspired me to push the boundaries of my knowledge and skills. I would also like to express my heartfelt appreciation to INOR USM for the research grants and financial support that catalyzed this research. Their dedication to scientific research has allowed me to explore new ideas and push the boundaries of knowledge in GaN HEMT power devices. I am also grateful for the research facilities, especially the simulation tools provided. I dedicate this thesis mainly to my parents, sisters, and grandmother in appreciation of their unwavering love, support, and understanding. Their unwavering confidence in my abilities and constant encouragement have been a beacon of light, and I am forever grateful to them for their sacrifices and for being my pillar of strength. I also genuinely thank all my colleagues and peers, especially Dr. Khairul Arshad, who have been integral during my academic journey. Our collaborations, camaraderie, and thought-provoking discussions have created a vibrant and supportive academic community. Also, the frequent intellectual engagement and words of encouragement have made this journey a truly enriching experience. Studying while working has been extremely challenging, especially during the COVID-19 times, hence I am thankful to my manager for allowing me to take breaks whenever I could, to concentrate on my studies. Finally, I sincerely thank all the individuals who have contributed to this thesis in various capacities, both directly and indirectly. Although their names may not be explicitly mentioned here, their contributions have been invaluable.

TABLE OF CONTENTS

ACKNOWLEDGEMENT	ii
TABLE OF CONTENTS	iii
LIST OF TABLES	vi
LIST OF FIGURES	viii
LIST OF SYMBOLS	xiii
LIST OF ABBREVIATIONS	xv
ABSTRAK	xvii
ABSTRACT	xviii
CHAPTER 1 INTRODUCTION	1
1.1 General Introduction	1
1.2 Problem Statements.....	4
1.3 Aim and Objectives	6
1.4 Originality of the Study.....	7
1.5 Scope of the Study.....	7
1.6 Thesis Outline	9
CHAPTER 2 LITERATURE REVIEW AND THEORETICAL BACKGROUND	10
2.1 Introduction	10
2.2 Fundamentals of AlGa _N /Ga _N HEMT.....	10
2.2.1 Device Structure and Parameters	10
2.2.2 Simulation-based Studies	14
2.3 Challenges and Issues in AlGa _N /Ga _N HEMT.....	15
2.3.1 Current Collapse, High Gate Leakage, and Electric Field	15
2.3.2 Advantages of normally-off operation	27
2.3.3 High Ohmic Contact Resistances	39

2.4	Summary	44
CHAPTER 3 METHODOLOGY.....		45
3.1	Introduction	45
3.2	Simulation Method.....	46
3.2.1	Coupling Equations	46
3.2.1(a)	Poisson Equation	46
3.2.1(b)	Electron Current Continuity Equation.....	47
3.2.2	Boundary Conditions.....	49
3.2.2(a)	Ohmic Contact.....	49
3.2.2(b)	Schottky Contact.....	50
3.3	Simulation Tool: COMSOL Multiphysics	52
3.3.1	Overview of the Simulation Tool.....	52
3.3.2	Simulation Flow of AlGaIn/GaN HEMT	53
3.3.3	Physics of Models: Semiconductor and Electrostatic	58
3.3.4	Discretization Formulation.....	59
3.3.5	Solver and Convergence.....	61
3.3.6	Assumptions made for validation.....	64
3.4	Summary	66
CHAPTER 4 RESULT AND DISCUSSIONS		68
4.1	Introduction	68
4.2	Model Validation.....	69
4.2.1	Validation Overview	69
4.2.2	Experimental and Simulation Setup.....	70
4.2.3	Results and Comparison.....	70
4.3	Influence of Trenches in AlGaIn/GaN HEMT	72
4.3.1	Device Description.....	72
4.3.2	Optimization of p-GaN doping and work function	74

4.3.3	Optimization of Trenches' Depth.....	79
4.3.4	Characterizations of Trenches-filled Structure	80
4.4	Influence of Notches in AlGaIn/GaN HEMT.....	88
4.4.1	Device Description.....	88
4.4.2	Electrical Characterizations.....	89
4.5	Influence of Graded Channel in AlGaIn/GaN HEMT.....	96
4.5.1	Device Description.....	96
4.5.2	Electrical Characterizations.....	99
4.6	Influence of p-GaN Gate Airgap in AlGaIn/GaN HEMT	102
4.6.1	Model Description.....	102
4.6.2	Influence of Device Geometry	103
4.6.3	Electrical Characterizations.....	110
4.6.4	Influence of Passivation Layers	113
4.7	Influence of Recessed p-GaN Gate in AlGaIn/GaN HEMT	117
4.7.1	Device Description.....	117
4.7.2	Always-off Operation.....	118
4.7.3	Ohmic Contact Resistances.....	120
4.8	Summary	124
CHAPTER 5 CONCLUSION AND RECOMMENDATION		128
5.1	Conclusion.....	128
5.2	Recommendations for Future Research	130
REFERENCES.....		131
LIST OF PUBLICATIONS		

LIST OF TABLES

		Page
Table 2.1	Material properties of GaN and AlGaN.	11
Table 2.2	Electrical comparison of GaN-based HEMTs with FPs.	21
Table 2.3	Properties of different high-k materials.	26
Table 2.4	Compilations of normally-off HEMTs with a p-GaN gate.	34
Table 2.5	Electrical characteristics for multi-barrier GaN HEMTs, based on recent literature. The threshold voltage (V_{th}) varied significantly with the Al composition and recessed-gated depth (H).	38
Table 2.6	Comparison of different metal stacks that form ohmic contact in HEMT.	42
Table 3.1	Basic properties of AlGaIn and GaN materials from the COMSOL Multiphysics database.....	48
Table 3.2	Overview of simulation with the corresponding solved equations. ...	48
Table 3.3	Comparison between the two types of metal contact.....	51
Table 3.4	Mesh sizes to cover all regions.	55
Table 3.5	Comparison of extracted data from Semiconductor and Electrostatics modules.....	59
Table 3.6	Comparison of discretization formulation in COMSOL.....	60
Table 3.7	Assumptions made for the validation.....	66
Table 4.1	Material properties used in the validation.....	70
Table 4.2	Material parameters of the devices.	73
Table 4.3	Properties of the materials used.	73
Table 4.4	Semiconductor models applied for the device simulation.	74
Table 4.5	Dimensions of the notches.	89
Table 4.6	Constant parameters defined for the simulated structure.....	97

Table 4.7	Dimensions of the simulated devices.....	103
Table 4.8	Updated gate dimensions with varied L_G	105
Table 4.9	Updated gate dimension with varied L_{GD}	107
Table 4.10	Properties of the dielectric materials.....	114
Table 4.11	Summary of Results and Discussions.	126

LIST OF FIGURES

	Page
Figure 2.1	Schematic of a typical AlGa _N /Ga _N HEMT, showing the Si substrate, Ga _N buffer layer, Ga _N channel layer, AlGa _N barrier layer, Si ₃ N ₄ passivation layer, and the source (S), gate (G), and drain (D) regions. The dimensions of each layer and contact spacing are also indicated.....12
Figure 2.2	Bandgap diagram of AlGa _N /Ga _N HEMT. This demonstrates the energy levels of the conduction bands, highlighting how the electrons are confined at the interface to form the 2DEG, which is a key feature of the HEMT's operation.13
Figure 2.3	An illustration of the current collapse mechanism.....16
Figure 2.4	An illustration of the virtual gate effect.17
Figure 2.5	(a) Schematic of an AlGa _N /Ga _N HEMT with FP structure and (b) Equivalent energy band profile. The configuration allows for improved breakdown voltage following the mitigation of current collapse.....20
Figure 2.6	The plots of (a) transfer, (b) transconductance, (c) drain leakage current, and (d) output characteristics for AlGa _N /Ga _N HEMTs with AlN layers.23
Figure 2.7	Band gap and permittivity relationships for various materials.25
Figure 2.8	(a) A normally-off AlGa _N /Ga _N HEMT with a p-type doped Ga _N and (b) Energy band diagram with the comparison between different layers, whereby the channel region's conduction band is displaced above the Fermi level.30
Figure 2.9	Electric field profile for an always-off AlGa _N /Ga _N HEMT at a drain bias of 300 V.31
Figure 2.10	An ideal depiction of the gate with a p-Ga _N gate layer.32

Figure 2.11	(a) Schematic of device structure with $L_{GS}/L_G/L_{GD}/W_G = 2/4/10/100 \mu\text{m}$ and (b) Transmission Electron Microscopy (TEM) image of the device.	36
Figure 2.12	Schematic of an E-mode HEMT with triple AlGaIn barrier layers....	37
Figure 2.13	Process flowchart for device etching with an ohmic groove in Ti/Al/Ti/Al/Ti/Al/Ti/Al/Ni/Au.....	43
Figure 3.1	The research methodology of this research.....	46
Figure 3.2	Energy band diagram of AlGaIn/GaN heterostructure, showing the conduction band discontinuity (ΔE_C), 2DEG formation, electric potential, and Fermi level (E_F).	48
Figure 3.3	Schematic of an AlGaIn/GaN HEMT configuration with the applied boundary conditions	51
Figure 3.4	Representation of a simulated 2D model of AlGaIn/GaN HEMT.	53
Figure 3.5	Representation of materials assignment to each device layer.....	54
Figure 3.6	Mesh refinement for the HEMT device	55
Figure 3.7	An example of simulated (a) $I_{DS}-V_{GS}$ and (b) $I_{DS}-V_{DS}$ characteristics using the COMSOL simulation tool.	56
Figure 3.8	Process flow diagram of AlGaIn/GaN HEMT simulation.	57
Figure 3.9	Transfer characteristics for models running on FEM Quasi-Fermi Linear and Quadratic formulation. The runtime for the latter is longer at 13 minutes and 29 seconds, compared to the former with only 3 minutes and 1 second.	61
Figure 3.10	Representation of convergence plots for (a) passing, and (b) failing HEMT simulations.	62
Figure 3.11	Representation of undefined values issue during computation.....	63
Figure 3.12	Representation of failures with no-convergence situations, denoted by (a) iteration count, and (b) computation error message.	64
Figure 4.1	Illustrations of the (a) fabricated device, and the $I_{DS}-V_{GS}$ plots for the (b) fabrication work, and (c) simulation validation.....	71

Figure 4.2	Illustrations of the (a) fabricated device, and the I_{DS} - V_{GS} plots for the (b) fabrication work, and (c) simulation validation.....	71
Figure 4.3	Schematics of the (a) C-HEMT and (b) TT-HEMT devices.....	72
Figure 4.4	Transfer characteristics of the TT-HEMT at $V_{DS} = 0$ V with varying p-GaN doping concentrations (N_P).	75
Figure 4.5	Transfer characteristics of the TT-HEMT at $V_{DS} = 0$ V with varying gate metal work functions of 4.1 eV, 4.5 eV, and 5.2 eV at a p-GaN doping density of (a) $1.0 \times 10^{18} \text{ cm}^{-3}$ and (b) $1.0 \times 10^{19} \text{ cm}^{-3}$	77
Figure 4.6	The (a) transfer and (b) breakdown characteristics of TT-HEMT at $V_{GS} = -1$ V with different trench depths of 10 nm, 15 nm, 20 nm, and 24 nm. No changes were observed in current density and V_{th} , but V_{BR} improved with depth optimization.	79
Figure 4.7	Electron concentration n_e (cm^{-3}) in the (a) C-HEMT and (b) TT-HEMT at $V_{DS} = 30$ V and $V_{GS} = -1$ V. The arrows denote the coupling of electron current density with their concentration.	80
Figure 4.8	(a) Output characteristics at $V_{GS} = -1$ V, and (b) transfer characteristics for both devices at $V_{DS} = 0$ V.....	81
Figure 4.9	(a) Electric field distribution of TT-HEMT at $V_{GS} = -1$ V with varying V_{DS} . Higher V_{DS} corresponds to higher peaks and average electric field. (b) Electric field distribution of C-HEMT and TT-HEMT devices along the channel ($y = 1.9 \mu\text{m}$) at $V_{DS} = 100$ V and $V_{GS} = -1$ V. As observed, the peak for TT-HEMT is lower at 1.8 MV/cm compared to 11 MV/cm of the conventional.	84
Figure 4.10	Electric potential distribution for the conventional and TT-HEMT devices along the channel ($y=1.9 \mu\text{m}$) with $V_{DS} = 100$ V and $V_{GS} = -1$ V. Overall, the potential for both devices is identical.....	85
Figure 4.11	Breakdown characteristics of the TT-HEMT and C-HEMT devices at $V_{GS} = -1$ V.....	86
Figure 4.12	Breakdown voltage comparison of the TT-HEMT with values from published works (Exp: experiment, Sim: simulation).....	87

Figure 4.13	Schematics of the (a) conventional, and (b) proposed HEMT with dual-notch.....	88
Figure 4.14	The (a) transfer characteristics of the conventional and dual-notch HEMT at $V_{DS} = 0$ V. (b) I_{DS} - V_{DS} characteristics for both devices at $V_{GS} = -1$ V and V_{DS} sweeps from 0 V to 12 V.	91
Figure 4.15	(a) Electric field distribution for the conventional design at $V_{GS} = -1$ V and varying V_{DS} . A higher voltage corresponds to higher peaks and overall distribution. (b) Electric field distribution between conventional and notch-filled design at $V_{GS} = -1$ V and $V_{DS} = 130$ V.	93
Figure 4.16	(a) Electric potential for notch-filled HEMT at $V_{GS} = -1$ V and varying V_{DS} . A higher drain voltage corresponds to a higher peak. (b) Electric potential for both designs at $V_{GS} = -1$ V and $V_{DS} = 100$ V.....	94
Figure 4.17	Breakdown voltage comparison between the conventional and dual-notch HEMT at $V_{GS} = -1$ V, with the latter achieving a higher breakdown voltage at 222.6 V.	95
Figure 4.18	Schematic of the graded AlGaIn/GaN HEMT.	97
Figure 4.19	Al concentration along the channel ($y = 2.525$ μ m), indicating an increase from 0.2 at the source region to 0.4 at the drain side.....	100
Figure 4.20	Electric field distribution in the conventional and graded AlGaIn/GaN HEMT along the channel ($y = 2.525$ μ m) at $V_{GS} = -1$ V and $V_{DS} = 60$ V.	101
Figure 4.21	Breakdown properties of both devices at $V_{GS} = -1$ V.....	102
Figure 4.22	Schematics of the (a) conventional and (b) airgap gate HEMT.....	103
Figure 4.23	The (a) transfer and (b) gate leakage characteristics at $V_{DS} = 0$ V, and (c) breakdown properties at $V_{GS} = -1$ V for the airgap-filled device with different L_G of 0.6 μ m and 1.0 μ m.	106
Figure 4.24	The (a) transfer and (b) gate leakage characteristics at $V_{DS} = 0$ V, and (c) breakdown properties at $V_{GS} = -1$ V for the airgap gate	

	HEMT with different L_{GD} values. The gate leakage current for 1.5 μm and 1.7 μm length is slightly higher, although the resulting breakdown also significantly increases, demonstrating the trade-off between them.....	108
Figure 4.25	The plots of (a) $I_{DS}-V_{GS}$, (b) $I_{GS}-V_{GS}$, and (c) breakdown properties with varied p-GaN thickness.....	110
Figure 4.26	(a) $I_{DS}-V_{GS}$ and (b) $I_{GS}-V_{GS}$ plots for both devices at $V_{DS} = 0$ V, denoting V_{th} of 0 V, and (c) $I_{DS}-V_{DS}$ plot of both devices at $V_{GS} = -1$ V.....	111
Figure 4.27	Breakdown properties of the conventional and airgap gate HEMT at $V_{GS} = -1$ V.	113
Figure 4.28	The (a) transfer and (b) $I_{GS}-V_{GS}$ plots when using different passivation materials. The peak drain current is highest when using Ga_2O_3 material, which shows a lower gate leakage current compared to ZnO, which has the lowest peak drain current.....	114
Figure 4.29	Schematic of the recessed-gate p-GaN HEMT.....	117
Figure 4.30	The simulated $I_{DS}-V_{DS}$ plot of the recessed p-GaN gate HEMT and conventional devices at $V_{DS} = 0.5$ V. Enhancement-mode HEMTs exhibit a sharp increase in I_{DS} with positive V_{th} values, while depletion-mode HEMTs show high I_{DS} at zero V_{GS} , which decreases with negative V_{GS}	118
Figure 4.31	Differences in doping profile between the two devices.	121
Figure 4.32	The (a) transfer and (b) gate leakage characteristics of both devices at $V_{DS} = 0.5$ V.	121
Figure 4.33	Output characteristics of both devices at $V_{GS} = -1$ V.....	122
Figure 4.34	Breakdown properties of both devices at $V_{GS} = -1$ V.....	124

LIST OF SYMBOLS

E_g	Bandgap
k_B	Boltzmann constant
V_{BR}	Breakdown voltage
ΔE_C	Conduction band offset
E_C	Conduction band edge
q	Charge of an electron
E_{crit}	Critical electric field
C_{ox}	Oxide capacitance
I_{DS}	Drain-source current
d_{eff}	Effective distance
L_{GD}	Distance between gate and drain
L_{GS}	Distance between gate and source
V_{DS}	Drain-source voltage
ΔE_V	Discontinuity of valence band
R_D	Drain contact resistance
k	Dielectric constant
$R_{DS,ON}$	Dynamic on-state resistance
m^*	Electron effective mass
E	Electric field
j_n	Electron current density
μ_n	Electron mobility
χ	Electron affinity energy
ψ	Electric potential

n_e	Electron concentration
L_G	Gate length
W_G	Gate width
V_{GS}	Gate-source voltage
I_g	Gate leakage current
μ_p	Hole mobility
N_A	Hole concentration
L_{FP}	Length of the field plate
$I_{d,max}$	Maximum drain current
ϕ_M	Metal work function
E_{peak}	Peak electric field
ϕ_n	Quasi-Fermi potential
ϵ_r	Relative permittivity
$I_{DS,sat}$	Saturation region of the drain current
N_C	State density of conduction band
V_{sat}	Saturation electron velocity
$I_{d,sat}$	Saturation current
R_S	Source contact resistance
ϕ_B	Schottky barrier height
R_{on}	Specific on-resistance
V_{th}	Threshold voltage
H_T	Trench depth
L_T	Trench length
E_V	Valance band edge
ϵ_o	Vacuum permittivity

LIST OF ABBREVIATIONS

Al	Aluminum
Al ₂ O ₃	Aluminum oxide
ALD	Atomic layer decomposition
AlGaN	Aluminum gallium nitride
AlN	Aluminum nitride
BJT	Bipolar junction transistor
Bi ₂ O ₃	Bismuth oxide
C-HEMT	Conventional high-electron-mobility-transistor
CMOS	Complementary metal-oxide-semiconductor
DIBL	Drain-induced barrier lowering
DLTS	Deep-level transient spectroscopy
D-mode	Depletion mode
E-field	Electric field
E-mode	Enhancement model
FEM	Finite element method
FET	Field-effect transistor
FVM	Finite volume method
FP	Field-plate
FNL	Floating Network License
GaAs	Gallium arsenide
GaN	Gallium nitride
Ga ₂ O ₃	Gallium oxide
Au	Gold
HEMT	High-electron-mobility-transistor
HfO ₂	Hafnium dioxide
HRiC	High-resistivity SiC
ICP	Inductively coupled plasma
IGBT	Insulated gate bipolar transistors
InP	Indium phosphide
ITO	Indium tin oxide
LCCT	Local charge compensation trench (LCCT)

LRSiC	Low-resistivity SiC
MISHEMT	Metal-insulator-semiconductor double heterojunction high electron mobility transistors
MOCVD	Metal-organic chemical vapour deposition
MOSFET	Metal-oxide-semiconductor field-effect transistor
Ni	Nickel
PDE	Partial differential equation
Pt	Platinum
SRH	Shockley-Read-Hall
Si	Silicon
SiO ₂	Silicon dioxide
Si ₃ N ₄	Silicon nitride
SiC	Silicon carbide
SCR	Silicon-controlled rectifiers
TEM	Transmission electron microscopy
TCAD	Technology Computer-Aided Design
Ti	Titanium
SnO ₂	Tin (IV) oxide
TT-HEMT	Triple-trench high-electron-mobility-transistor
2D	Two-dimensional
2DEG	Two-dimensional electron gas
3D	Three-dimensional
TRIACS	Triodes for alternating current
UWBG	Ultra-wide bandgap
WBG	Wide bandgap
ZnO	Zinc oxide
ZrO ₂	Zirconium dioxide

PENAMBAHBAIKAN REKA BENTUK STRUKTUR HEMT BERASASKAN ALGAN/GAN UNTUK PERANTI KUASA BERPRESTASI TINGGI

ABSTRAK

Penyelidikan ini memberi tumpuan kepada pengenalan reka bentuk struktur inovatif untuk menangani pelbagai cabaran yang berkaitan dengan AlGa_N/Ga_N HEMTs. Simulasi terlebih dahulu disahkan menggunakan data eksperimen bagi memastikan kebolehpercayaannya. Struktur yang dikaji dikategorikan kepada dua bahagian: di bawah dan di atas kawasan get. Bagi menangani kepekatan medan elektrik tinggi berdekatan dengan sisi sentuhan logam, tesis ini mencadangkan variasi struktur baharu di bawah get, termasuk parit, takik, dan saluran terged AlGa_N, yang melibatkan variasi komposisi Al sepanjang saluran dalam lapisan AlGa_N. Pendekatan ini mengoptimumkan taburan medan elektrik dan mengurangkan kemungkinan runtuh arus melalui peningkatan mobiliti. Tumpuan lain adalah kebolehpercayaan get, khususnya kebocoran get dan rintangan operasi keadaan hidup melalui reka bentuk di atas get, seperti rongga udara get yang direka melalui pemisahan fizikal antara sentuhan logam dan bahan semikonduktor. Pengoptimuman lanjut melibatkan ketebalan lapisan p-Ga_N, kepekatan doping p-Ga_N, dan saiz peranti, untuk menyeimbangkan prestasi dan kebolehpercayaan. Ini termasuk analisis bagi tukar ganti dalam kepanjangan get, variasi ruang get-salur, dan bahan penapisan permukaan untuk pengurangan arus kebocoran get, manakala get p-Ga_N turut direka untuk operasi keadaan hidup. Secara keseluruhan, peningkatan sebanyak 478% dalam sifat keruntuhan dan 403% dalam arus salir maksimum telah dicapai dengan saluran terged. Penemuan ini menjanjikan kemajuan dalam elektronik pengguna dan aplikasi industri, seterusnya menyumbang kepada landskap peranti kuasa global.

IMPROVEMENT OF STRUCTURAL DESIGN OF ALGaN/GaN BASED HEMT FOR HIGH PERFORMANCE POWER DEVICES

ABSTRACT

This research focuses on the introduction of innovative structural designs aimed at addressing the multifaceted challenges associated with AlGaN/GaN HEMTs. Simulations are first validated against experimental data to ensure reliability. The investigated structures are then categorized into two; below and above the gate region. To address the high electric field concentrations near the metal contact edges, this thesis proposes new structural variations below the gate, which includes triple-trench, dual-notch, and an AlGaN-graded channel with varied Al composition along the channel. These approaches optimize the electric field distribution and reduce the likelihood of current collapse through enhanced mobility. Another focus is gate reliability, particularly gate leakage and on-state resistance through designs above the gate, such as a gate airgap, created by physically separating the metal contact from the semiconductor. Further optimizations include p-GaN layer thickness, p-GaN doping concentration, and device dimensions, balancing performance and reliability. This includes a comprehensive analysis of the trade-offs in gate length, gate-drain spacing, and surface passivation materials to reduce gate leakage, and a recessed p-GaN gate is also developed for safer on-state operation. Overall, a 478% improvement in breakdown properties and a 403% increase in maximum drain current have been realized with the graded channel. The findings offer promising advancements in consumer electronics and industrial applications, contributing to the global power devices landscape.

CHAPTER 1

INTRODUCTION

1.1 General Introduction

Power devices, which control the flow of electrical energy in diverse applications, are crucial parts of electrical energy. These devices transform and regulate electrical power, ensuring efficient operation and energy savings across diverse uses, from consumer electronics to industrial machinery [1]. Power devices come in various types, each serving specific functions. Diodes, for instance, are fundamental in converting alternating current (AC) to direct current (DC) by allowing current to flow in only one direction. Meanwhile, thyristors are used to control high power and are frequently found in industrial motor drives, light dimmers, and pressure control systems. These also include silicon-controlled rectifiers (SCRs) and triodes for alternating current (TRIACS) [2]. Bipolar Junction Transistors (BJTs) are also utilized in amplification and switching applications, handling higher currents than field-effect transistors (FETs), making them suitable for power amplification. Field-effect transistors (FETs), particularly metal–oxide–semiconductor field-effect transistors (MOSFETs), are also essential in power conversion and signal amplification owing to their high efficiency and fast switching capabilities. Additionally, insulated gate bipolar transistors (IGBTs) combine the high-efficiency switching of MOSFETs with the high-current handling capability of BJTs, making them widely used in high-power applications like inverters for electric vehicles (EVs) and renewable energy systems [3].

Recent years have witnessed significant advancements in power device development, improving their performance and reliability with the focus shifted more towards wide bandgap (WBG) semiconductors such as silicon carbide (SiC) and

gallium nitride (GaN) [4-5]. These materials offer superior properties, including higher breakdown voltage, better thermal conductivity, and faster switching speeds than traditional silicon (Si). In particular, GAN has gained attention due to its potential to enable more compact and efficient power devices [6]. Current research in power devices aims to overcome the constraints of traditional Si-based devices by leveraging the advantages of these WBG semiconductors. Developing new semiconductor materials with better electrical and thermal properties, innovating new device structures to improve performance and reliability, improving heat dissipation techniques to ensure device longevity, and integrating power devices with other parts to create more compact and efficient systems are some of the main research areas [7]. This integration research explores monolithic integration and advanced packaging techniques [8].

Compared to their Si equivalents, GaN-based power devices, such as GaN MOSFETs, GaN HEMTs, and GaN Schottky diodes, have significant advantages, including higher operating power, with lower leakage currents and higher efficiency. Their high thermal conductivity also contributes to efficient heat dissipation, improving the performance and reliability of devices, particularly in high-power applications [9]. They also exhibit high electron mobility and saturation velocity, making them ideal for high-frequency applications. The significantly faster switching speed of GaN transistors, up to 30 times faster than silicon counterparts, combined with reduced on-resistance, results in enhanced efficiency by minimizing power losses, enabling the use of smaller passive components, and facilitating overall system miniaturization [10].

GaN-based power devices are widely used in different fields, including power conversion, to reduce device size and improve efficiency in power supply systems,

specifically in DC-DC converters, AC-DC converters, and inverters. GaN's high-frequency performance in RF and microwave amplifiers is also crucial for wireless communication infrastructure, radar systems, and telecommunications. The material's resilience also makes them perfect for high-reliability uses in the military and aerospace industries, where they are employed in communication and power control systems. In consumer electronics, GaN devices are increasingly found in fast chargers and power adapters, offering compact and efficient solutions [11].

The shrinking of electronic systems has also been significantly impacted by the rapid development of Ga. Its superior properties enable the development of compact power devices that can deliver great performance in a smaller footprint, which is in line with the growing demand for smaller, more efficient devices [22]. This is particularly important in applications such as portable electronics and electric vehicles, where space and weight are critical design considerations. The advancement of GaN technology is expected to play a pivotal role in enabling the next generation of compact, high-performance power devices. As global energy consumption continues to rise, there is an urgent need for technologies that can reduce energy losses and improve overall efficiency [23]. GaN's unique properties, including its ability to handle high power densities and operate reliably under challenging conditions, make it ideal for high-power applications such as renewable energy systems, where efficient power conversion is essential to maximize energy output and minimize losses [21].

The possibility of improved longevity and reliability is another driving force for the study of GaN power devices. GaN's inherent material properties, such as its resistance to high temperatures and radiation, make it well-suited for demanding applications where long-term reliability is crucial. This includes aerospace and defense applications, where devices must operate reliably under extreme conditions [24].

However, despite its vast potential, several challenges persist that hinder the full realization of its benefits within HEMTs, particularly for AlGaIn/GaN-based heterostructures. One significant issue is the optimization of the device structure to enhance performance parameters, with conventional designs frequently having issues with reliability and electrical performance under high-power conditions [25].

Implementing GaN-based HEMTs holds significant potential for advancing the electronics and telecommunications industries, with further potential for improved performance and efficiency. Among these are electric vehicles, in which the race to lead in the electric vehicle market remains competitive following the world's transition to electric transportation [12]. GaN HEMTs can also be used in EV powertrains, including motor drives and onboard chargers, to improve energy efficiency and reduce the overall weight of the vehicles, thus enhancing their performance and range. Additionally, GaN-based power devices can significantly enhance the efficiency of solar inverters and wind turbine converters in renewable energy systems. Higher power conversion efficiencies can be achieved, which is crucial for maximizing the output of renewable energy installations [13]. Hence, the potential future applications of GaN HEMTs are vast, and ongoing research is focused on improving device performance, reliability, and integration. This includes exploring new structural variations, such as optimizing layer thickness, to achieve further enhancements [14].

1.2 Problem Statements

The growing demand for efficient, reliable, and high-performance power devices drives continuous advancements in power electronics, particularly for applications requiring high power densities and frequencies [15]. AlGaIn/GaN HEMTs are promising candidates due to their high electron mobility, breakdown voltage, and thermal conductivity. However, achieving these benefits requires overcoming

significant challenges, such as achieving uniform material quality in terms of crystal structure, defect density, doping concentration, and surface morphology. Consistent device performance, particularly in terms of current handling, voltage stability, and reliability, is difficult to achieve due to the precise control required over the growth and processing conditions [16]. As GaN does not require external doping, its electrical characteristics must be carefully optimized by controlling intrinsic properties, such as carrier concentration and mobility. Achieving a carrier concentration in the range of mid- 10^{17} to mid- 10^{20} , is crucial to ensure sufficient current flow, while maintaining high mobility reduces conduction losses. Excessive carrier concentrations can increase scattering and degrade mobility, impacting performance. Therefore, precise growth and doping processes are crucial for optimizing these parameters in GaN devices designed for high-power applications [17].

In AlGaN/GaN HEMTs, critical issues like current collapse, caused by traps and surface states that disrupt carrier flow, remain significant which impact device performance [26-27]. These traps critically influence carrier dynamics and overall device functionality, leading to issues such as current degradation and reduced breakdown voltage. Additionally, high electric field concentrations near the gate also often lead to premature breakdown and reliability concerns, emphasizing the need for effective field management [28]. Previous efforts have explored strategies like field plates, surface passivation, and optimized doping profiles, which have shown promise but remain insufficient to address all challenges comprehensively. Structural variations, such as novel dielectric materials, optimized barrier thicknesses, and advanced gate engineering, offer potential solutions, but their effects are not fully understood and require further investigation [29]. Therefore, innovative structural

designs must be explored to address these challenges effectively and enhance device performance.

A thorough literature review reveals gaps in understanding the effects of structural variations on HEMT performance. Experimental methods, while valuable, are constrained by fabrication variability and the difficulty of isolating individual phenomena. In contrast, simulation-based research provides a controlled platform for investigating the fundamental physics of traps, allowing detailed analysis of their interaction with electric fields and carrier concentrations. Simulations not only clarify the mechanisms underlying critical performance metrics, such as current degradation and breakdown voltage, but also provide actionable insights to guide experimental validation, minimizing costly and time-consuming fabrication iterations. This study focuses on innovative structural variations, including dual-notches, triple-trenches, and optimized doping profiles, to address these critical issues. By filling these gaps, this study aims to enhance AlGaIn/GaN HEMT performance and reliability, advancing power electronic technology.

1.3 Aim and Objectives

This study aims to address the issues associated with AlGaIn/GaN HEMTs through innovative structural variations. The objectives include:

1. To design new structures below the gate region with trenches, notches, and an AlGaIn-graded channel for minimization of the high electric field and current collapse.
2. To investigate the effect of gate leakage and always-off operation following structural modifications above the gate region with a p-GaN gate airgap, recessed p-GaN gate, and surface passivation.

3. To analyze the impact of structural variations on electrical performances via maximum drain current and breakdown voltage.

1.4 Originality of the Study

The originality of the study can be summarized as follows:

1. Innovative designs with triple-trench and dual-notch.
2. Implementation of a new p-GaN gate structure with an airgap.
3. A novel graded channel design.
4. Increment of 403% for maximum drain current.
5. 478% improvement in breakdown voltage.

Through these contributions, this study aims to advance the state of AlGaIn/GaN HEMT technology, addressing key challenges and paving the way for broader commercial applications.

1.5 Scope of the Study

This study focuses on the simulation of AlGaIn/GaN HEMTs, utilizing an advanced simulation tool with COMSOL Multiphysics to examine the physical and electrical properties of the devices. The procedures involve key steps such as setting up the geometric structure, defining material properties, applying boundary conditions, and solving equations to simulate device behavior. The simulations employ multiple physics modules to examine charge transport, field distributions, and electrical characteristics.

To ensure model accuracy and reliability, the study involves thorough validation of the simulation results by comparison with empirical data from existing literature. This validation step establishes a solid foundation for further research and development. Building upon these validated models, the study explores innovative

structural modifications to enhance device performance and reliability. Specifically, new structures below the gate region featuring trenches, notches, and an AlGaIn-graded channel were developed to minimize high electric fields and mitigate current collapse. Additionally, implementing a recessed p-GaN gate, a p-GaN gate airgap, and different surface passivation layers above the gate region explores the consequences of gate leakage and on-state operation. The study thoroughly analyzes the impact of these structural variations on electrical performance, mainly on the maximum drain current and breakdown properties. It also systematically investigates various layer sizes, compositions, doping concentrations, and structural configurations to identify optimal design parameters. By rigorously examining these modifications, the research aims to uncover improved design concepts for the devices.

This study is limited to the use of undoped GaN within the AlGaIn/GaN HEMT structure and does not extend to other material systems or doped configurations. The simulations are primarily confined to two-dimensional (2D) models to balance complexity with computational feasibility. The research is also limited to a full simulation approach, excluding any experimental fabrication, material growth processes, and physical characterization techniques. While the focus is on the electrical characteristics of the devices, thermal management, mechanical stress, RF performance, and related aspects are outside the scope of this study. By delineating these specific boundaries, such as optimizing carrier concentration, the research provides a clear and systematic approach. Using COMSOL simulations, it focuses on precise modeling of device physics and structural variations to address critical challenges in GaN-based HEMTs, including mitigating current collapse, reducing gate leakage, enhancing breakdown voltage, and improving reliability under high-power conditions. The findings are expected to contribute significantly to the advancement

of power electronic technologies, offering valuable insights for the development of next-generation power devices.

1.6 Thesis Outline

This thesis is divided into five chapters, structured as follows: **Chapter 1** presents a brief introduction to GaN-based power devices and HEMTs, including their applications. The study's problem statements, research objectives, originality, and thesis scope have also been described. **Chapter 2** delves into the literature overview of existing AlGaIn/GaN HEMTs research. It includes device and material properties of the HEMTs, their fundamental principles, known issues that limit performances, and structural solutions associated with the devices. **Chapter 3** details the methodologies used in this study, including the coupling methods, boundary conditions, and the simulation flow with COMSOL Multiphysics. It also discusses the semiconductor and electrostatic models and the characterization techniques used to evaluate device performance. **Chapter 4** presents the discussion of the results, including validation of the simulated models followed by electrical characterization with structural variations, mainly trenches, notches, an airgap, an AlGaIn-graded channel, and a recessed p-GaN gate. Various device optimization effort for improved electrical performance is also discussed, such as varied doping concentrations, device sizes, and materials. **Chapter 5** summarizes the research findings and provides recommendations for future research.

CHAPTER 2

LITERATURE REVIEW AND THEORETICAL BACKGROUND

2.1 Introduction

Aluminum gallium nitride/gallium nitride (AlGaN/GaN) high-electron-mobility transistors (HEMTs) have garnered significant attention in recent years due to their superior material properties, making them suitable for high-power, high-frequency, and high-temperature applications. This chapter provides an overview of the fundamentals, challenges, and issues related to AlGaN/GaN HEMTs, serving as a foundation for understanding the current state of research in this field. It starts with the basic device structure and operating principles, highlighting how the heterojunction between AlGaN and GaN layers creates a two-dimensional electron gas (2DEG), crucial for high electron mobility. Major challenges including current collapse, gate leakage, high electric field, normally-on operation, and high ohmic contact resistance were discussed, along with proven solutions from the literature. By integrating recent research findings, this chapter provides a comprehensive and up-to-date overview of AlGaN/GaN HEMTs to clarify complex concepts and highlight advancements.

2.2 Fundamentals of AlGaN/GaN HEMT

2.2.1 Device Structure and Parameters

AlGaN/GaN HEMT technology provides unparalleled current density and output power, positioning itself as a leading choice for various applications. These devices benefit from a wide energy band gap, high critical electric field, and robust thermal dissipation capabilities, making III-nitride compound semiconductors a focal point of research for electronic devices. The intrinsic properties of nitride-based semiconductors support low on-state resistance, high off-state voltage, and substantial power density [30].

Within power device applications, GaN-based configuration typically shows superior performance compared to those based on gallium arsenide (GaAs), silicon (Si), and silicon carbide (SiC), with the former offering enhanced input power robustness, a saturation electron velocity (v_{sat}) that is at least twice as fast as that of silicon (Si) and GaAs, and a dielectric field strength (E_c) that is significantly greater than Si and 7.5 GaAs [31-32]. This results in GaN-based HEMTs outperforming Si-based HEMTs, delivering higher output power and operating frequencies. Table 2.1 presents the typical properties of AlGaN and GaN used in HEMT design [33].

Table 2.1 Material properties of GaN and AlGaN.

Parameters	Unit	Al _{0.25} Ga _{0.75} N	GaN
Electron mobility (μ_n)	cm ² V ⁻¹ s ⁻¹	300	1200
Energy band gap (E_g)	eV	3.87	3.43
Conduction band density of state (N_c)	10 ¹⁸ cm ⁻³	2.74	2.24
Valance band density of state (N_v)	10 ¹⁹ cm ⁻³	1.98	2.51
Saturation velocity (V_{sat})	10 ⁷ cm s ⁻¹	1.10	2.50
Relative permittivity (ϵ)	-	8.80	8.90

A typical AlGaN/GaN HEMT configuration comprises heterojunction formation following the alignment of wide band gap semiconductors adjacent to each other, as shown in Figure 2.1 [34]. Above the AlGaN layer, the gate metal forms a Schottky contact, which controls the polarization charge density at the AlGaN/GaN interface, and the source and drain, which form the ohmic contact. Although not permanently, the electrons will cluster near the AlGaN layer, which acts as a barrier due to its higher band gap. As a result, a two-dimensional electron gas (2DEG) forms in the GaN layer, close to the AlGaN/GaN border [35]. The quality of the 2DEG, in terms of its density, carrier mobility, and interface abruptness, is critical for device

performance. These factors are influenced by the growth method, substrate material, and doping level in the carrier supply layer, as they directly impact conductivity, scattering, and the overall efficiency of the device.

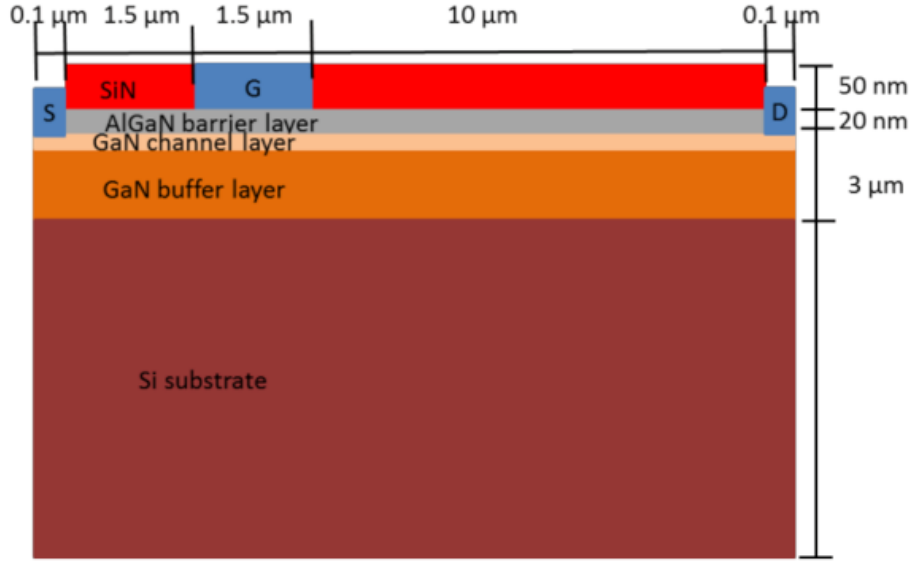


Figure 2.1 Schematic of a typical AlGaN/GaN HEMT, showing the Si substrate, GaN buffer layer, GaN channel layer, AlGaN barrier layer, SiN passivation layer, and the source (S), gate (G), and drain (D) regions. The dimensions of each layer and contact spacing are also indicated.

Unlike GaAs-based devices, GaN HEMTs do not require doping to achieve a high electron concentration in the channel [36]. Instead, carriers are generated due to the polarization mismatch between the AlGaN and GaN layers, driven by both piezoelectric and spontaneous polarization. Consequently, the 2DEG density in GaN HEMTs is significantly higher than other heterostructure configurations, such as indium phosphide (InP) or GaAs-based devices, influenced by the intrinsic physical characteristics of the materials involved. The polarization-induced 2DEG density ($n_{2\text{DEG}}$) can be expressed as [37]:

$$n_{2\text{DEG}} = \frac{P_{\text{piezo}} + P_{\text{spont}}}{q} \quad (2.1)$$

where P_{piezo} is the piezoelectric polarization, P_{spont} is the spontaneous polarization, and q is the electron charge. As implied, the total polarization-induced 2DEG density results from piezoelectric and spontaneous polarizations, which lead to the accumulation of electrons at the AlGa_N/Ga_N interface, forming a high-density 2DEG. As previously implied, the conduction band edge of the Ga_N layer is lower than that of the AlGa_N barrier layer, with this energy difference (ΔE_C) facilitating electron transfer into the Ga_N layer, where they are then confined, forming a high-density 2DEG. The difference in energy is also known as conduction band offset (ΔE_C), described as [38]:

$$\Delta E_C = E_{C,\text{AlGa}_N} - E_{C,\text{Ga}_N} \quad (2.2)$$

where E_{C,AlGa_N} and E_{C,Ga_N} are the conduction band edges of AlGa_N and Ga_N, respectively. The bandgap diagram in Figure 2.2 visually represents the conduction band offset (ΔE_C) between the AlGa_N and Ga_N layers [39].

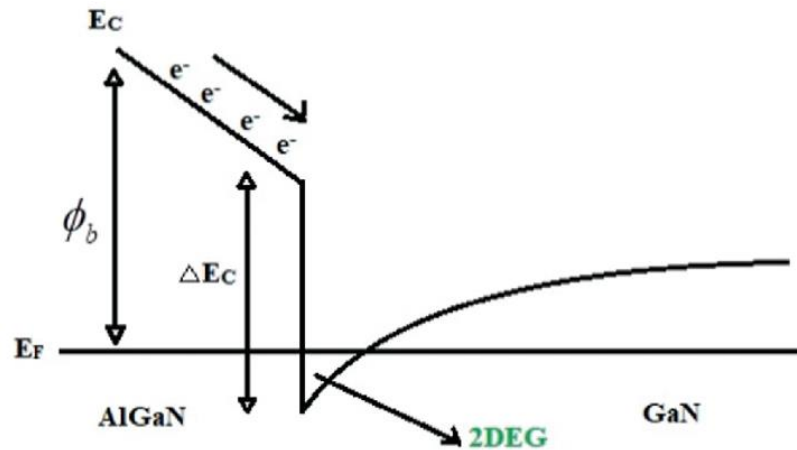


Figure 2.2 Bandgap diagram of AlGa_N/Ga_N HEMT. This demonstrates the energy levels of the conduction bands, highlighting how the electrons are confined at the interface to form the 2DEG, which is a key feature of the HEMT's operation.

Recent studies have reported high Al composition in AlGa_N channels exceeding 0.4, with some cases reaching up to 0.5 or higher, due to their ability to

enhance critical breakdown voltage and electric field distribution [40]. While typical Al composition in AlGaN is typically lower than 0.3, higher compositions have been shown to enable higher voltage operations due to the enhanced critical electric field (E_{crit}), denoted by [41]:

$$E_{\text{crit}} = \frac{2 V_{\text{BR}}}{d} \quad (2.3)$$

where V_{BR} is the breakdown voltage, and d is the source-drain spacing. This enhancement is due to the wider bandgap and stronger polarization effects associated with increased Al content, which improve the channel's ability to manage electric field stress effectively. Planar ohmic connections have been identified for HEMT heterostructures with an Al composition exceeding 50% in the AlGaN channel, although the specific contact resistivity also degrades with higher Al concentration [42]. This characteristic is particularly appealing for the development of UWBG semiconductor devices, owing to the polar nature of III-nitride materials [43].

2.2.2 Simulation-based Studies

Simulation tools are essential for designing and optimizing AlGaN/GaN HEMTs through the exploration of various device structures, understanding underlying physical phenomena, and prediction of device performance under different operating conditions. Among these tools, Technology Computer-Aided Design (TCAD) tools, such as Silvaco and Synopsys, have been predominantly used due to their specialized capabilities for semiconductor device simulation [44]. However, COMSOL Multiphysics has also been employed for its versatility and comprehensive physics modeling capabilities [45].

For electrical and thermal simulations which are crucial for understanding the performance of AlGaN/GaN HEMTs under various biasing conditions, COMSOL's

module allows detailed modeling of charge transport, electric fields, and current flow. For instance, Alam et. al [46] conducted thermal simulations with COMSOL to analyze the impact of low-cost substrates on the performance of AlGa_N/Ga_N HEMTs. Their results highlighted that low-cost substrates, while economically advantageous, often exhibit higher lattice mismatch and lower thermal conductivity compared to premium substrates like SiC or sapphire. This mismatch increases defect density, impacting the formation and quality of the two-dimensional electron gas (2DEG), while lower thermal conductivity hinders heat dissipation, raising the junction temperature during high-power operation. These trade-offs emphasize the challenges in balancing material cost and performance. Similar work is also possible with TCAD tools, including the one by Palazzo et. al [47] who used Synopsys TCAD to investigate the maximum junction temperature of HEMT devices.

Despite its versatility, the use of COMSOL for AlGa_N/Ga_N HEMT simulations remains less prevalent than specialized TCAD tools like Silvaco and Synopsys [48]. The adoption of TCAD tools for extensive semiconductor device simulations is more mature, offering advanced features for modeling complex semiconductor processes and phenomena. As a result, most research in the power device field utilizes TCAD tools for detailed device simulations, leaving COMSOL-based studies relatively limited [49-50].

2.3 Challenges and Issues in AlGa_N/Ga_N HEMT

2.3.1 Current Collapse, High Gate Leakage, and Electric Field

One of the critical challenges for Ga_N HEMTs is the development of current collapse or dynamic on-state resistance ($R_{DS,ON}$) dispersion [51]. This issue occurs when hot electrons in the channel become trapped in various regions, such as the buffer layer, the AlGa_N layer, the passivation layer, or the interfaces between these layers, as

illustrated in Figure 2.3 [52]. This trapping reduces the channel carrier density, leading to an increase in resistance and a subsequent decrease in drain current. The phenomenon is primarily attributed to traps in the GaN buffer layer, which are often related to structural defects in the GaN materials.

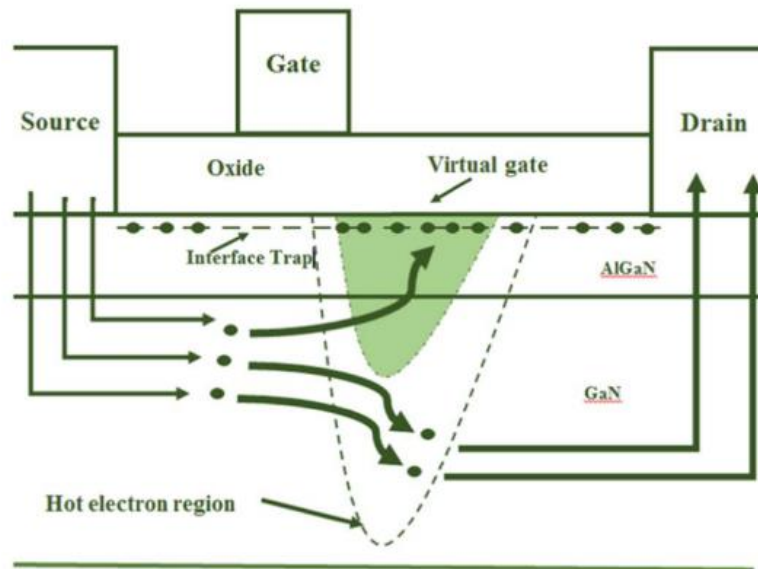


Figure 2.3 An illustration of the current collapse mechanism.

The formation of a virtual gate is a significant factor contributing to the current collapse. This virtual gate forms between the gate and drain terminals due to trapped charges in the AlGaN layer or at the AlGaN/passivation interface, as shown in Figure 2.4 [52]. The virtual gate effectively increases the gate-to-drain capacitance and modifies the electric field distribution within the device, which can slow down current transients when the gate and drain voltages are adjusted rapidly. This phenomenon, known as gate lag and drain lag, manifests as an increase in $R_{DS,ON}$ and significantly impacts the device's reliability and performance [53].

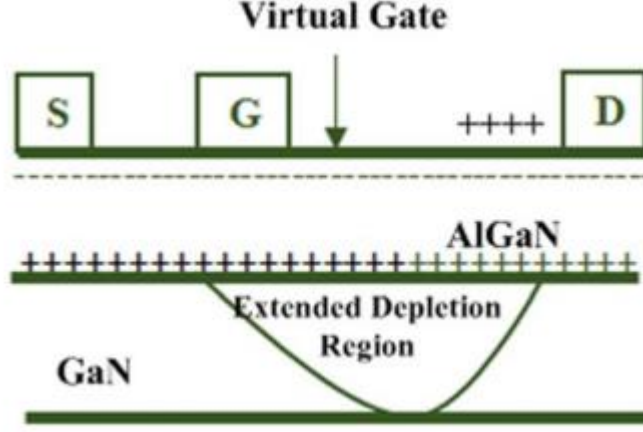


Figure 2.4 An illustration of the virtual gate effect.

Studies have shown that the traps can be formed due to various factors, including nitrogen vacancies resulting from plasma damage during processing, dislocations at material interfaces, or unintended doping in the GaN layer. These traps capture carriers, which can cause changes in the threshold voltage and decrease peak transconductance [54]. Capacitance and conductance analyses have also suggested the presence of traps at the AlGaN/GaN interface and under the gate [55]. The current collapse phenomena due to trapped states can be modeled by an exponential decay equation [56-58]:

$$I_{collapsed} = I_0 \exp\left(-\frac{t_{trapping}}{\tau_{trapping}}\right) \quad (2.4)$$

where $I_{collapsed}$ is the collapsed current due to trapping, I_0 is the initial current before any trapping occurs, $t_{trapping}$ is the time over which trapping occurs, and $\tau_{trapping}$ is the characteristic trapping time constant. This equation indicates that the current decreases exponentially over time as more carriers become trapped. The impact of trapping on the drain current (I_D) can be quantified by [56-58]:

$$I_D = I_{D0} \left(1 - \frac{N_t}{N_{total}}\right) \quad (2.5)$$

where I_{D0} is the drain current without trapping, N_t is the number of trapped carriers, and N_{total} is the total number of carriers. This equation implies that as more carriers get trapped (N_t increases), the drain current (I_D) decreases, with the fraction N_t/N_{total} representing the proportion of carriers that are trapped out of the total available carriers.

Meanwhile, gate leakage current is another critical parameter of GaN HEMTs, directly influencing their performance and reliability. This phenomenon refers to the undesired flow of current through the gate dielectric or the Schottky barrier when a voltage is applied to the gate [60]. Forward gate leakage current restricts the gate voltage swing, which results in power losses, while reverse gate leakage leads to off-state power consumption and a reduced breakdown voltage. Setting the Schottky gate to a reversed bias can mitigate the potential power loss by switching off the drain current. The gate leakage current (I_G) can be explained as follows, derived from both the thermionic emission model and applied gate voltage [61-62]:

$$I_G = A^*T^2 \exp\left(-\frac{q\phi_B}{kT}\right) \left(\exp\left(\frac{qV_G}{kT}\right) - 1\right) \quad (2.6)$$

where A^* is the Richardson constant, T is the temperature, ϕ_B is the Schottky barrier height, q is the electron charge, k is Boltzmann's constant, and V_G is the gate voltage. This expression is relevant for situations of high thermal energy, such as Schottky barriers at higher temperatures. Meanwhile, the Fowler-Nordheim tunneling equation would be more appropriate for modeling leakage under high electric fields, as later explained in Equation (4.25).

A high peak electric field, typically occurring near the gate during high-bias operation, presents additional challenges. These may facilitate charge trapping between the passivation layer and the III-nitride interface, where electrons become

trapped in free surface states under a strong electric field, triggering virtual gating and current collapse. Devices with smaller gate-drain spacing, scaled down for high-speed operation, are particularly susceptible to significant current collapse, amplifying the virtual gating effect of surface traps, as shown in the following expression [62-63]:

$$E = \frac{V_{DS}}{L_{GD}} \quad (2.7)$$

where E is the electric field, V_{DS} is the drain-source voltage, and L_{GD} is the gate-drain spacing. Hence, managing the electric field distribution between the gate and drain is crucial for achieving a higher breakdown voltage per channel length. The presence of active electron traps between the gate and drain significantly decreases with the peak electric field, even resulting in reduced current collapse and knee walkout [64].

As solutions, researchers have explored various mitigation plans, such as field plate (FP) implementation, gate structure variations, and surface passivation strategies. The FP refers to an extension of the gate towards the drain contact in which a metallization layer is deposited atop the passivation layer of the device, as illustrated in Figure 2.5 [65]. This leads to a reduced peak electric field near the gate. This effectively increases the total distance from L_{GD} , with electric field distribution with field plate (FP) now becomes [62][66]:

$$E_{FP} = \frac{V_{DS}}{L_{GD} + L_{FP}} \quad (2.8)$$

where L_{FP} is the length of the field plate extension, L_{GD} is the gate-drain spacing, and V_{DS} is the drain-source voltage. The electric field distribution profile improves as the depletion region broadens with the FP, creating multiple peaks instead of a single one, which results in a more uniform electric field distribution. This implementation also

helps reduce the reverse gate leakage current following an extra surface for field line termination, thereby mitigating electrical field congestion near the gate.

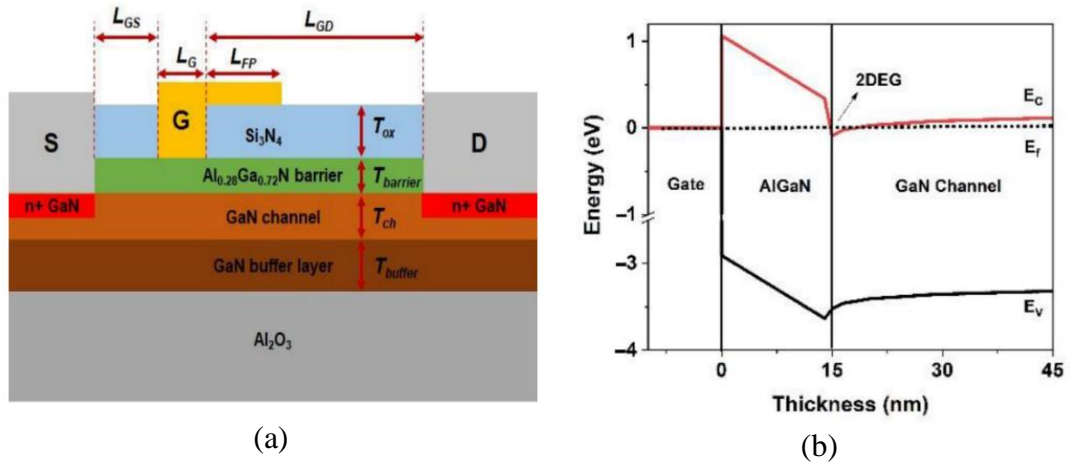


Figure 2.5 (a) Schematic of an AlGaN/GaN HEMT with FP structure and (b) Equivalent energy band profile. The configuration allows for improved breakdown voltage following the mitigation of current collapse.

Consequently, various architectures of HEMTs with field plates (FPs) have been further developed for optimized performances. For instance, Zhang et al. [67] discovered that FP technology can introduce a novel charge-balancing effect in lateral power devices. Additionally, Wong et al. [68] designed a GaN HEMT with an innovative asymmetric slant FP, achieving a high breakdown voltage of 146 V, aiming to increase the breakdown voltage without enlarging the device size. This outcome aligns with the study by Chen et al. [69], which indicated that potential dispersion near the drain edge increased with rising source voltage due to the escalating electric field between the gate and drain areas. Near the standard FP edge, there was a significant potential rise, resulting in an extremely high electric field of 4.8 MV/cm. Kabemura et al. [70] also observed improvements in breakdown voltage using short- and moderate-length FPs on HEMTs. Recent findings on the characteristics of HEMTs with FP are summarized in Table 2.2, underscoring the importance of optimizing the devices' sizes for enhanced performance and reliability.

Table 2.2 Electrical comparison of GaN-based HEMTs with FPs.

L_{FP} [μm]	L_G [μm]	L_{GD} [μm]	Passivation Layer	Cap Layer	f_T [GHz]	Electric Field [MV cm^{-1}]	V_{th} [V]	$g_{m,max}$ [mS mm^{-1}]	$I_{ds,max}$ [mA mm^{-1}]	V_{BR} [V]	Ref.
0.67	0.26	2.00	SiN	-	41.00	0.71	0.65	780.0	1060	138	[68]
1.75	0.40	-	SiN	-	40.00	-	-4.30	434.8	2160	872	[71]
			HfO ₂	-	28.00	-	-	434.0	2110	912	
0.60	0.70	-	SiN	-	-	-	-	-	-	150	[72]
0.90	0.25	2.70	SiN	GaN	20.00	17.00	-	270.0	760	330	[73]
2.00	3.00	22.00	-	-	-	3.00	-	-	-	2200	[74]
1.00	0.25	2.70	SiN	AlN/GaN-	-	2.90	0.50	175.0	900	291	[75]
1.50	1.50	5.00	Si ₃ N ₄	-	-	-	-4.00	70.0	310	970	[65]
2.00	2.00	15.00	SiN	GaN	-	-	-3.50	138.0	-	365	[76]
3.00	1.00	8.00	SiN	-	19.00	4.87	-	-	3400	376	[77]
0.30	0.30	1.50	SiN	-	-	2.70	-5.84	-	-	400	[78]
0.80	0.50–1.00	3.55	Si ₃ N ₄	-	6.70	-	-2.683	58.0	~100	669	[79]
0.20	0.25	2.70	SiN	GaN	28.30	-	-	350.0	1000	254	[80]
0.10	0.25	2.70	SiN	GaN	28.00	1.80	-	314.0	820	342	[81]
0.50	0.25	2.70	SiN	GaN	47.07	-	-4.30	323.0	1080	298	[82]
0.75	0.2	1.35	SiN	-	62.40	-	-2.60	-	1000	140	[83]
0.30	0.23	1.00	SiCN	-	-	-	-	-	-	282	[84]
0.80	0.25	1.00	SiN	-	38.00	-	-3.30	58.7	-	127	[85]

As shown in Table 2.2, several FP HEMTs also incorporate a GaN cap layer, which helps to mitigate self-heating effects and current collapse. This thin layer also protects the AlGaIn surface from oxidation and provides an additional barrier at the Schottky contact, ultimately reducing leakage current. The effect of the cap layer on the thermal conductivity (κ) can be mathematically expressed as [86]:

$$\kappa = \frac{Q}{A \cdot \Delta T \cdot d} \quad (2.9)$$

where Q is the heat flow, A is the cross-sectional area, ΔT is the temperature difference, and d is the thickness of the material. A thicker cap layer corresponds to a higher area, hence lower thermal conductivity.

The GaN cap-filled devices can be further improved with a high-resistivity variant, which is believed to further improve electric field distribution and breakdown capability, given the reported high breakdown voltage (V_{BR}) of 1020 V [87]. Nirmal et al. explored this concept further by adding a thin AlN layer between the SiN and GaN layers, as shown in Figure 2.6 [88-89]. The addition of the AlN layer serves several purposes: its superior thermal conductivity (2 W/cm·K) significantly enhances heat dissipation, and reduces lattice mismatch at the SiN/GaN interface, mitigating defect generation and improving structural integrity. The AlN layer also acts as an effective barrier against meltback etching during device fabrication and minimizes charge trapping at the SiN/GaN interface, leading to better electrostatic control, reduced current collapse, and improved device reliability. These benefits are reflected in the results, which showed a 6.26% increase in drain current, a 14% higher breakdown voltage, and a 10% reduction in current collapse compared to the conventional design, highlighting the effectiveness of this modification.

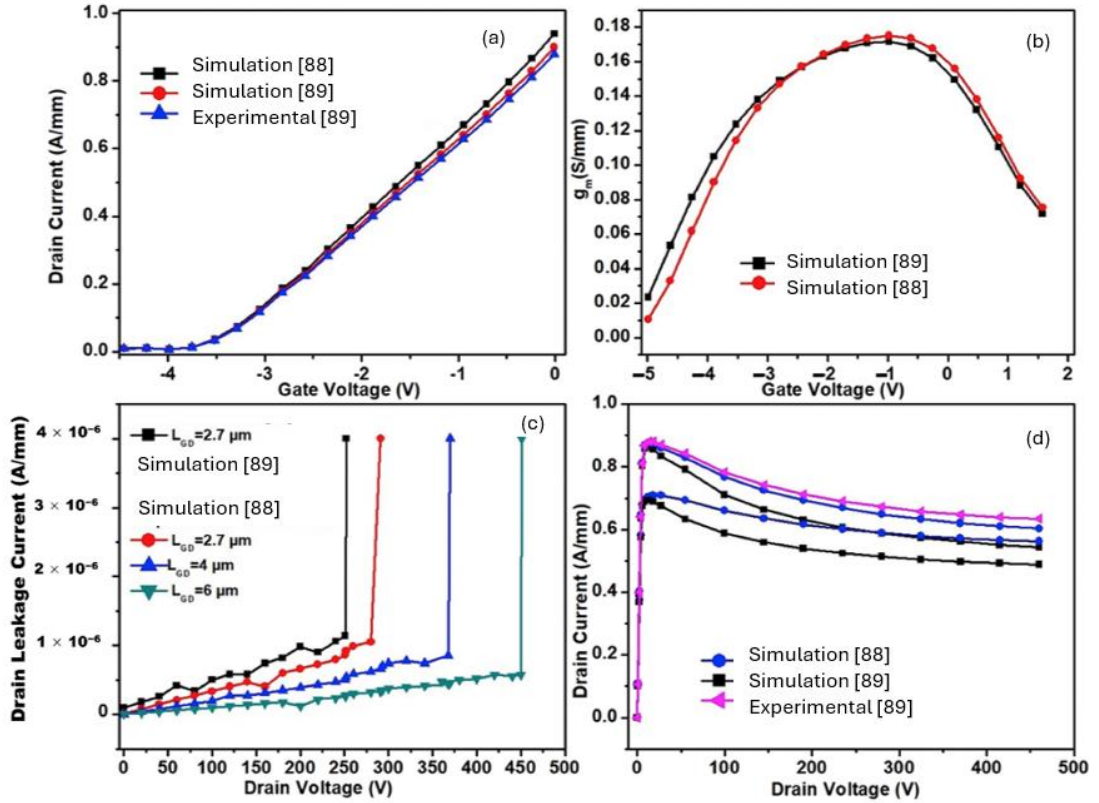


Figure 2.6 The plots of (a) transfer, (b) transconductance, (c) drain leakage current, and (d) output characteristics for AlGaN/GaN HEMTs with AlN layers.

FP-HEMTs are also typically in contact with a surface passivation layer (PL) made of nitride or oxide to prevent electron leakage through high-density shallow surface traps. Another reason is to protect the device surface from environmental contaminants, such as moisture and oxygen, which can lead to oxidation and degradation over time. Using materials with excellent insulating properties and high permittivity, such as silicon nitride (SiN), surface passivation can be formed through the MOCVD method [90]. Hence, by passivating the surface, the layer reduces the density of these states, minimizing their impact on carrier mobility and device stability. The reduction in surface states can be quantified using the following relation for surface recombination velocity (S) [91-92]:

$$S = S_0 \exp\left(-\frac{E_t}{kT}\right) \quad (2.10)$$

where S_0 is the initial surface recombination velocity, E_t is the trap energy level, k is Boltzmann's constant, and T is the temperature. This equation indicates that the surface recombination velocity decreases exponentially with trap energy level (E_t), which increases following passivation. In other words, higher trap energy levels make it less likely for carriers to recombine, thus reducing the recombination velocity. Further, PL effectively reduces the density of surface states, which translates to a decrease in S_0 , by providing a cleaner surface with fewer defects. Lower recombination velocities lead to higher carrier lifetimes and mobility, resulting in better performance of HEMTs and less degradation over time.

The electrical properties typically vary depending on the surface passivation materials. There is a correlation between band gap and permittivity for materials widely used as passivation layers, as illustrated in Figure 2.7 for their trade-offs [93]. Given the significant difference in permittivity between high- k dielectrics and AlGaN, electric flux is transmitted more effectively from the semiconductor surface. For instance, aluminum oxide (Al_2O_3), with its higher permittivity of around 9 compared to SiO_2 , offers better surface passivation by reducing electric field peaks and distributing them more uniformly. Further, its high bandgap (approximately 8.7 eV) provides significant chemical and thermal stability, hence enhancing the electrical performance.